Bioprinting 20 (2020) e00091

Contents lists available at ScienceDirect

Bioprinting

journal homepage: www.elsevier.com/locate/bprint

Research paper

Additive manufacturing enables production of de novo cardiomyocytes by controlling embryoid body aggregation

Rupambika Das, Javier G. Fernandez *

Singapore University of Technology & Design, 8 Somapah Road, 487372, Singapore

ARTICLE INFO

Keywords:
Additive manufacturing
Cellular differentiation
Geometric cues
Cardiogenesis
Embryonic stem cells
Embryoid body

ABSTRACT

Embryonic stem cells act as a valuable and promising resource in the field of regenerative cell-based therapies and in studying various developmental models. These derived cells can be induced in vitro to differentiate into numerous distinct cell lineages by the formation of Embryoid Bodies (EBs), in a process strongly conditioned by the geometrical characteristics of the EB. This artificial conditioning of cellular differentiation is performed using tools prioritizing geometrical definition but lacking versatility for the adaptation of the geometry to different conditions. Here we demonstrate the production of cardiomyocytes by using high definition direct writing technologies to influence EB aggregation from stem cells. We gauged the impact of this technology over the standard known methods in terms of size dispersion, cell packing density, cardiac tissue health, and the number of cardiomyocytes produced. The feasibility to create small variations of a geometry enabled optimizing EB formation for cardiogenesis and its threefold increase with respect to traditional techniques. This result highlights how the fast-paced improvement of geometrical control in additive manufacture might hold the key to unprecedented control of stem cell differentiation for regenerative medicine.

1. Introduction

The production of engineered tissue in vitro for diagnostics, research, and regenerative therapies requires the use of cells with functionality like that of the targeted natural tissue. The main accomplishments in this field have come from the use of primary cells; however, this strategy is limited by the availability of the targeted cells and their mitotic potential. This is particularly significant for those cells building central organs and withdrawn from the cell cycle, such as those in brain and heart [1,2]. The limited regenerative function of cardiac cells [3,4] not only denies the heart a natural healing process that occurs in other organs, but it also hampers the development of biomedical therapies. As a result, myocardial infarction continues to be one of the most devastating diseases worldwide, affecting approximately 17% of the population [5,6]. After an infarction, the wounded region does not recover naturally, instead it begins a process where dysfunctional myocytes are gradually replaced by inert collagenous scar tissue [7]. Because of the heart's inability to restore the functionality of its damaged cardiac tissue, heart transplantation continues to be the gold standard treatment [8] to restore a severely damaged heart.

In the last decade, attention has shifted to the use of stem cells (SCs), as a (theoretically infinite) source of functional cardiomyocytes [9]. SCs could enable the production of cardiac tissues for each patient, potentially providing the large amounts of cells needed for therapies that could not be derived directly from an adult heart. However, this promising therapeutic approach is limited by our ability to control the differentiation of SCs into the targeted tissue lineage [10,11].

Guided differentiation sequence for SCs both in vitro and in vivo requires a well-defined cell-cell communication. As oviparous animals demonstrate, these interactions are enough to fully determine cell differentiation and to direct the entire development of an embryo without the need of exogenous factors. Embryos undergo cell differentiation into three germ layers soon after gastrulation that later develop into various organs [12]. This phenomenon is replicated in the laboratory through the formation of the three-dimensional (3D) cell aggregates known as embryoid bodies (EBs), which mimic the cell-packing conditions found in developing embryos. While largely uncontrolled, the formulation of these aggregates strongly influences the differentiation of SCs; EB parameters such as size [13], shape [14], and density [15] have shown a direct correlation with the lineage of mature cells [16]. Currently, EBs are produced by aggregating cells in hanging drop cultures, suspension cultures, aggrewell plates [17,18] and bioreactors [19], where they

* Corresponding author.
E-mail address: javier.fernandez@sutd.edu.sg (J.G. Fernandez).

https://doi.org/10.1016/j.bprint.2020.e00091
Received 19 March 2020; Received in revised form 16 June 2020; Accepted 20 July 2020

spontaneously differentiate in a myriad of cell lineages from which specific cell types are later isolated [20]. While the product of these different techniques might look optically similar, they are separated in those producing EBs (e.g. hanging drop) and those producing "differentiating aggregates" (e.g. Aggrewell plates) [21]. In the case of EB's it refers to a population of stem cells forming a structure similar to an embryo in geometry (i.e. spherical) but also with similar cell-cell interaction. As a result, EB's can be handled as a unit and when placed on cell culture plates, they attach and grow sprouting from the EB. Differently, "differentiating aggregates" are produced to be differentiated chemically, they generally are not spherical, and have low internal cohesiveness. As a result, they break apart and disperse into smaller pieces and individual cells when moved to culture plates.

With the potential to produce any targeted cell type from a population of SCs, it is not surprising to see the growing interest in controlling the aggregation of SCs into EBs as a method to drive differentiation. Still, despite the remarkable advances made in the field, the ultimate goal of achieving highly homogeneous EBs has not been obtained [22]. However, the latest advances in additive manufacturing may have unlocked the tools necessary to reach a new level of control in directed differentiation of SCs, allowing us to achieve a greater level of accuracy and uniformity required in EB aggregation.

We demonstrate the potential of additive manufacturing by comparing results to those achieved by traditional methods across different cell population sizes. Cardiomyocytes generated by 3D printed devices with features across several dimensions with relevance for cell differentiation, as well as its application to produce the most efficient non-chemical cardiogenesis to date, triplicating the standard are analyzed in terms of their functionality, showing a remarkably high beating frequency and amplitude. Interestingly, the unprecedented versatility of the proposed system enabled to us determine for first time cell density and total number of cells as independent critical factors for cardiac differentiation. In contrast with current technologies, the proposed technology has a low manufacturing cost, is easily automated, highly versatile and enables the control of parameters such as EB density and aggregation times, which are outside the boundaries of what traditional techniques can attain.

2. Materials and methods

2.1. Embryonic stem cell culture

ES-E14TG2a was purchased from ATCC, USA. This cell line was procured from the inner cell mass of mouse embryo. To maintain pluripotency, the cells were cultured on 0.1% gelatin (Sigma Aldrich, USA) coated tissue culture plates in a supplemented growth medium. The media constituents were DMEM (Nacalai Tesque, Japan), 15% FBS (Gibco, USA), 1% Sodium Pyruvate (Thermo Fisher Scientific, USA), 1% L-Glutamax (Thermo Fisher Scientific, USA), 1x non-essential amino acids (Thermo Fisher Scientific, USA), 0.1 mM 2-β Mercaptoethanol (Thermo Fisher Scientific, USA), and 1000 U/ml Leukemia Inhibiting Factor (LIF) (LIF was added prior to use) (Life Technologies, Thermo Fisher, USA). The cultures were incubated at 37 °C and 5% CO2. The medium was changed every other day, and the cells were dissociated into single cells by 0.25% Trypsin-EDTA (Nacalai Tesque, Japan) every 2–3 days.

2.2. 3D printing and mold fabrication

PDMS free-standing device was fabricated by mimicking the mold printed by Objet 30 Prime Poly-inkjet (Stratasys) 3D printer, based on the principle of photolithography. The dimensions of the device were 22 × 22 mm, with micro-wells of 300 μm diameters. After printing, the molds were thoroughly washed and soaked in de-ionized water for 2 h and baked at 60 °C for 24 h. After mold fabrication, PDMS (Sylgard 184, Dow Corning) in ratio 10:1 was poured and cured at 60 °C for 24 h. The cured PDMS device was then soaked in 70% EtOH and sonicated for 15 min, followed by UV exposure for 30 min to ensure complete sterilization before using the device for experiment.

2.3. EB formation by the hanging drop method

After two days of passage, the cells were prepared for the experiment. The SCs were detached, centrifuged, and a cell count was taken to have 7000, 17,000, 44,000, and 570,000 cells in 20 μl of media. LIF was removed from the media to ensure differentiation. The calculated number of cells was added in a drop-wise manner on the cover of a non-adherent petri dish. The petri dish was flooded with PBS to prevent evaporation of the drops containing cells. The whole set up was then placed in the incubator at 37 °C with 5% CO2 and was undisturbed for two days (Day0 - Day2). After two days, the free-standing aggregate of EBs were transferred to an adherent 24 well-plate, and the media was switched every other day.

2.4. EB formation by the fabricated device

ES cells were detached, centrifuged, and re-suspended to a cell count of 7000, 17,000, 44,000, and 570,000 cells in 30 μl of media. LIF was removed from the media to ensure differentiation. The calculated cell number was then slowly dropped into the micro-well of 300 μm. All the devices with different cell count were centrifuged at 1000 rpm for 3 min. Following centrifugation, another 10 μl of media was added to the well. The six well-plate containing the devices were added with 1 ml of media to prevent evaporation of the media from the wells containing cells. The devices were then placed in the incubator at 37 °C and 5% CO2, undisturbed for two days (Day0 - Day2). Media was changed every day throughout the incubation period. After two days, the EBs were extracted and transferred to an adherent 24 well-plate for further differentiation.

2.5. Analysis of beating cells

All sequences of images were analyzed using the Image Processing toolbox of MATLAB (Mathworks). To identify the beating centers of the specific areas, the region and the sub-region of interest were defined in terms of number of frames and frame rate prior to evaluation of the mean contraction in x-y direction, along with the number of beats per min using the code and algorithms developed at the University of California at Berkeley by Nathaniel Huebsch and co-workers. The heat maps obtained were then used to analyze the health of the heart tissue formed after ten days of differentiation.

2.6. Immunohistology

The cells from both the methods are fixed with 4% paraformaldehyde for 15 min followed by permeabilization with 0.1% Triton X-100 (Nacalai Tesque, Japan). The next step was to block the cells with 5% BSA for 60 min at room temperature. The blocked cells were then incubated with primary antibody anti OCT-4 and alpha sarcomeric actinin (1:200) (Life Technologies, Thermo Fisher) prepared in 5% BSA overnight at 4 °C. The next day, the cells were incubated with secondary antibody conjugated with Alexa Fluor 546 (1:500) and Alexa Fluor 488 (1:500) (Life Technologies, Thermo Fisher) for 60 min at room temperature, followed by staining with a nuclear probe 4′, 6-diamidino-2-phenylindole-2HCl (1:1000) (Life Technologies, Thermo Fisher) for 2 min. Washing steps included 5 min each (three washes) with 1X-PBS after each chemical treatment. Imaging the cells was performed using Carl Zeiss (Fluorescence Inverted Microscope, Axio Observer). The images obtained were quantified by calculating the ratio between the number of bright pixels from the immunostaining and the DAPI signals. A normalization between correlated images was performed using the background signals, calculated on the void areas of the image. Due to the large datasets and to ensure the quality of the data, the tails fo the distribution

were removed by discarding pixels with brightness at more than one at one sigma of the mean brightness (i.e. remaining approximately 68% of the dataset) [23].

2.7. Flow cytometry

The efficiency of differentiation was quantified by using flow cytometry. At day 10 of differentiation the cells were washed with 1X PBS, dissociated using 0.25% trypsin and then fixed with 4% PFA in rocking condition for 10 min at room temperature. After incubation, the cell pellet was subsequently washed with 1X PBS and permeabilized with 0.1% Triton X-100. Following permeabilization, the cells were incubated with primary antibodies for 45 min, washed twice with 1X PBS, and finally incubated with secondary antibody for another 45 min. For flow analysis, cells were washed with two times with PBS and re-suspended in 1X-PBS. The primary antibody used was anti-sarcomeric alpha actinin (1:200) (Life Technologies, Thermo fisher) and secondary antibody used was Alexa Fluor 546 (1:500) (Life Technologies, Thermo fisher). Analysis was performed using the MACSQ (Miltenyi Biotec).

2.8. Scanning electron microscopy

The EBs extracted from the device and hanging drops were separately extracted and fixed with 4% paraformaldehyde for 10 min, followed by washing with 1X PBS for 10 min. The EBs were then gradually dehydrated by treating them with a series of ethanol concentrations. The gradient followed was 50% ethanol for 5 min, 70% ethanol for 10 min, 80% ethanol for 10 min, 90% ethanol 5 min, three times each, and finally 100% ethanol for 5 min, three times each. The dehydrated EBs were morphologically analyzed using SEM (JEOL JSM-7600F).

3. Results and discussion

3.1. Device Fabrication

Past studies have successfully demonstrated higher cardiomyocyte generation from EBs of diameters 300–400 μm [24] along with a strong impact of EB packing density in cardiac differentiation [15]. Despite this known influence of cell packing density and EB size aggregation on the differentiation pattern, these parameters are yet to regulated in a controlled manner. Variances in the diameter of EBs as low as a few micrometers lead to a significant difference in the lineage composition [25], a value well above the territory of standard hanging drop [26] and aggrewell well plates [27] aggregation methods.

Therefore, due to the lack of independent control of the parameters determining EB characteristics (i.e., shape, size, and density), EBs produced by traditional techniques result in aggregates of broad and uncontrolled geometries, diameters, and densities. This enables to study the influence of cell aggregation on the resulting tissue lineage, but not the other way around, where cell aggregation itself could be used as a tool to direct differentiation. The emergence of digital design, fabrication technologies, and their development of smaller and more accurate features may have unlocked the capability to accurately control stem cell differentiation via EB formation. Following this idea, we fabricated an aggregation device using high-precession poly-inkjet printing [28,29] with a specific focus on controlling the de novo synthesis of cardiomyocytes from a population of murine-derived embryonic stem cells (Fig. 1A). We selected mESC as the cellular model based on the ethical and technical factors necessary to produce this proof-of-concept studies, and as a platform before moving into depth studies with hESC and in vivo models (Further discussion on the cell model is in the supplementary information). The printer has nominal horizontal and vertical resolutions of 42 μm and 16 μm, respectively, within the range of single-cell dimensions [30].

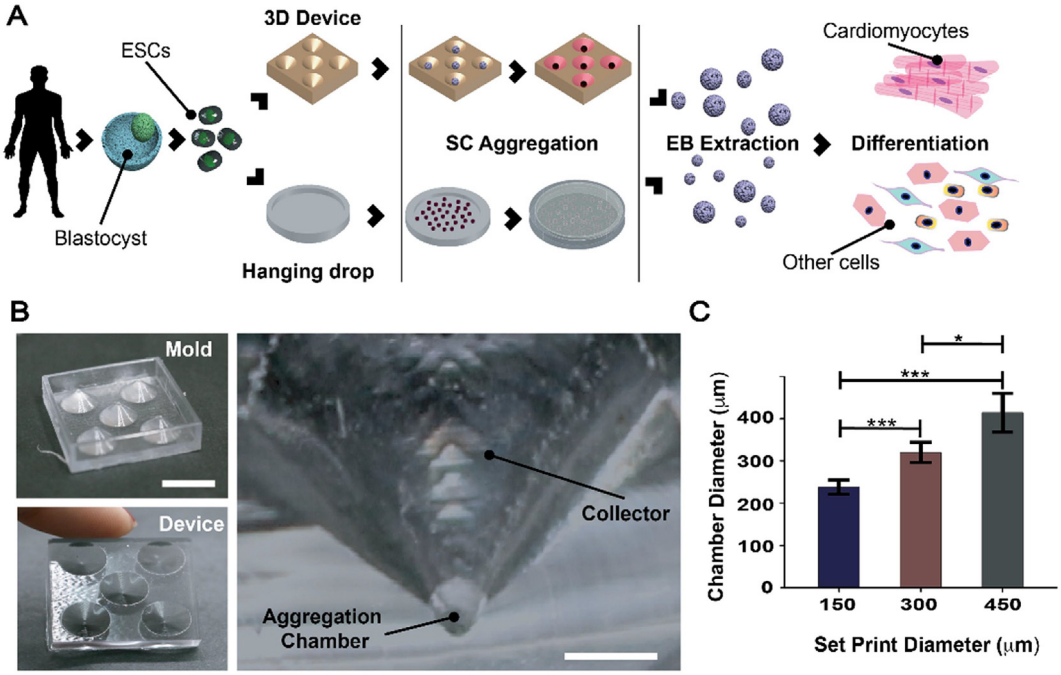

Fig. 1. Device Fabrication using a 3D printer. (A) Schematic representation of the experimental flow, showing the 3D printed device and hanging drop approaches adopted in this study for Embryoid Body formation. A comparison with commercial solutions is provided in the supplementary information (B) Pictorial representation of the fabricated micro-aggregation device along with the PDMS mold (Scale:13 mm). The PDMS mold was further horizontally dissected to clearly depict the different parts as well as the printed diameters of the structures (Scale: 23 mm). (C) Graphical representation of the statistical evaluation of the obtained print diameter of the device chamber in comparison to the set parameters.

The proposed micro-device consists of a funnel-like structure to collect and channel the SC population into a semispherical chamber of a predefined diameter (Fig. 1B). This aggregation chamber ultimately defines the size and geometry of the EB, serving as a selective tool for specific differentiation pathways. In contrast to the traditional technologies for the production of microelectromechanical systems, such as focused ion beam, chemical etching, or photolithography, poly-inkjet printing enables large volume (i.e., of several cm^3) manufacturing at resolutions with biological relevance in feasible times. It also allows the printing of a few dozen features in a single fabrication process, creating 3D molds containing different dimensions, such as micrometers (e.g. aggregation chamber), several millimeters (e.g. collector), and centimeters (e.g. device). 3D printing the aggregation devices enabled design flexibility, reduced cost, limited wastage of the materials, less assembling, improved sturdy quality along with the ability to reuse the molds. Every single print goes a long way which reduces the continuous need to purchase templated plates to form EBs. In the study for the proof of concept only 5 wells were printed but this can be scaled up to formulate over hundreds of EBs at a single shot. The printing time per device takes about 5 min with a high resolution providing the uniform surface finish. The printed devices require minimum post-processing, thereby making the whole fabrication system quite reliable and scalable [31].

To avoid exogenous influences on cell differentiation from the material, the 3D printed device was replicated in polydimethylsiloxane (PDMS), a silicone elastomer known for its chemical and biological inertness, lack of toxicity, and biocompatibility [32], as well as its ability to be further modified locally [33]. Three devices with aggregation chambers similar to optimal EBs for certain lineage differentiations [24] were manufactured and then digitalized by white light interferometry [34]. The resulting devices had spherical aggregation chambers of

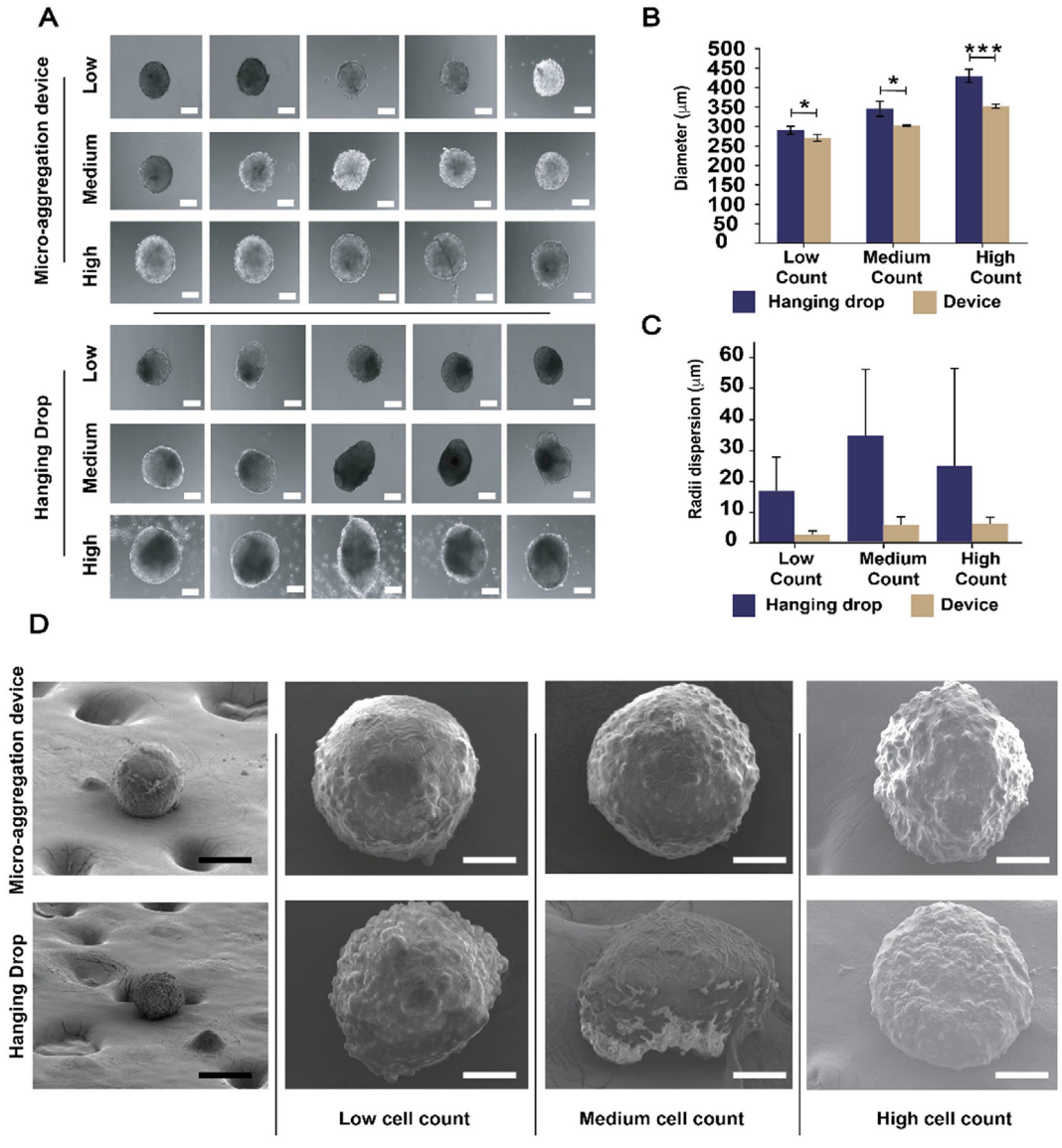

Fig. 2. Characterization of the Embryoid Bodies. (A) EB's extracted from the micro-aggregation device and hanging drop cultures on Day 2 containing different density of cells (Scale: 200 μm) (B) Statistical relevance of EBs extracted from the micro-aggregation device and hanging drop method was calculated after extraction on Day 2 to strike a co-relation between the cell density and cell packing efficiency. (C) Roundness calculated for the extracted EBs from both the techniques along with the statistically drawn relevance. (D) Morphological characterization of the EBs using Scanning Electron Microscope. (Row 1) Representation of an EB formed in a micro-aggregation device. An overall view of the EB (Scale: 200 μm) followed by the pictures depicting EBs formed from different cell number i.e. low, medium and high cell count (Scale: 50 μm). (Row 2) Representation of an EB formed by hanging drop cultures. Similar pattern followed as mentioned above. The overall view of the EB (Scale:200 μm) followed by the pictures depicting EBs formed from different cell number i.e. low, medium and high cell count (Scale: 50 μm) (Data from aggrewell plate is provided in Supplementary Figs. S1–S4).

diameters 237.6 ± 19.8, 319.3 ± 27.1, and 414.6 ± 49.7 μm and an average divergence of 47 μm with respect to the digital model, which is in agreement with the tool specifications (Fig. 1C). Larger aggregation chambers, which resulted in devices with negligible interest for guided differentiation, were also produced and characterized (Supplementary Fig. S3, S7 and S9).

3.2. Embryoid body formation

Based on previous results and our own observations, we focused the study on the formation of EB with controlled sizes to increase the net production of cardiomyocytes [35]. Using an aggregation chamber of 319.3 μm, we evaluated the formation of EBs of different densities by packing 7000 (low count), 17,000 (medium count) and 44,000 (high count) cells in the same volume. The number of cells was determined by the average number of cells in an EB of 319.3 μm formed by hanging drop and V-shaped wells (medium count), those cells in EBs of half volume (low count), and the number of cells in EBs of twice volume (high count).

For consistency with the control experiments, EBs were removed from the device after two days of incubation, as is the standard protocol for traditional techniques. This aggregation time is chosen based in the nutrient availability in a drop of cell media, a limiting factor of the hanging drop and V-shaped wells techniques. Whereas, this is not a limiting factor in the proposed system, because the media is stored in the collector and can be changed without disrupting the cell population in the aggregation chamber. This feature could enable the study of factors such as long aggregation times and use of exogenous factors at different time points in the aggregation, a limitation seen in traditional techniques.

Two days of incubation in the device resulted in EBs of diameters 270 ± 10, 302 ± 03, and 352 ± 06 μm (Fig. 2A) for low, medium and high cell counts, respectively. In contrast, those produced by hanging drop with the same cell counts had diameters of 290 ± 11, 345 ± 20, and 429 ± 18 μm (Fig. 2A), respectively, showing a size dispersion twice larger and half packing density (Fig. 2B) (Supplementary Fig. S4) results similar to those previously reported for this technique [36]. Concurrently, Aggrewell plates™ 400 were also considered to form cell aggregates. Aggrewell plates being commercially available are highly used to obtain numerous "differentiating aggregates" of cells that later are chemically driven into a specific fate in presence of particular growth medium. The extracted aggregates from the Aggrewell plate measured 131 ± 10.87, 143 ± 30.89 and 154.71 ± 16.39 μm (Supplementary Fig. S1) for low, medium and high count with evidenced high dispersion rates between experiments (Supplementary Table S2 and Supplementary Fig. S2) and with no statistically significant different sizes between aggregates of various cell counts (Supplementary Fig. S4). This result evidenced the suitability of these plates to perform satisfactorily in their standard conditions, but also their inability to be tailored for other conditions (i.e. different cell numbers, densities, or diameters). Aggrewell plates are preferable for largescale production of aggregates for chemical differentiation, where factors like precise EB diameter, morphology and cell count are not taken into consideration. In addition, being a technique focused on chemically induced differentiation, aggregates formed with Aggrewells differ from EBs on their cohesiveness. The lack of strong cell-cell interactions resulted on the aggregates breaking into smaller constructs and individual cells before attaching to a Petri dish, avoiding their use for non-chemical differentiation [37].

These acquired results highlight the efficiency of this new method and device design to control the diameter of EBs, a paramount criteria for non-chemical differentiation [38]. This provides a tool to achieve a remarkably high packing density in EBs.

The control and reproducibility of cell aggregation by the proposed system is not limited to an improved consistency on the average diameter of the EBs; it also enables the control of the geometry of the EB, a parameter out the scope of traditional techniques (Fig. 2C) (Supplementary Fig. S4) shows the typical geometrical variability of EBs from traditional techniques compared to those produced with the 3D printed chip. The EBs from the device were calculated to have higher degree of roundness, with a variance of the radii in each EB of 3.06, 6.75, and 6.64 μm for low, medium, and high cell counts, respectively. In contrast, the radii of those EBs formed by hanging drop showed a radii variability of 17.1, 35.1, and 25.3 μm for the same cell counts. To confirm roundness of the EBs rather than their circularity (i.e., a 2D dimensional disc), the geometry of the EBs was characterized by scanning electron microscopy (SEM) to confirm the spherical shape as well as an unusually even surface for EBs produced within the aggregation chamber (Fig. 2D).

3.3. Cardiomyogenesis

To measure the ability of the proposed system to influence the differentiation outcome of the SC population, the extracted EBs were cultured for ten days on an adherent surface. Pluripotency and cardiogenesis were simultaneously measured by the expression of OCT-4 and α-Sarcomeric Actinin at days 2, 5, and 10 (Fig. 3A) (Supplementary Fig. S6), respectively. As expected, cardiac markers were negligible in the early stages of differentiation, while pluripotency was at a maximum at that point. By day 5, the number of cells showing potential differentiation dropped an average of 42% with respect day 2; at day 10, there were no traces of undifferentiated cells observed (Fig. 3B). The differentiation of the stem cells is also noted as an increasing population of de novo cardiomyocytes. This process, however, seems to be slower at early stages of differentiation, while accelerates after day 5 (Fig. 3C). This lack of direct correlation between the differentiation of the stem cell population and the appearance cardiomyocytes might be due to the lack of α-Sarcomeric Actinin in immature cardiomyocytes after differentiation [39].

EBs aggregated in the conditions imposed by the aggregation chamber showed a three-fold increase in the number of cardiomyocytes produced when compared to hanging drop method (Fig. 3D) for the same cell number. The EBs considered for the quantification of the total number of cardiomyocytes produced were separate from the set of EBs taken for measuring the differentiation pattern. Therefore, enabling us to better understand speed the appearance of cardiomyocytes versus efficiency of cardiogenesis. The percentage of cardiomyocytes in the 302 μm diameter EBs reached 1.75%, in comparison to the 0.40% maximum efficiency reached by the hanging drop method—which is, to our knowledge, the most efficient de novo cardiomyocyte production to date based on aggregation control without electrical or chemical stimulation. The maximum peak for cardiomyocyte production from EBs of different characteristics was not found to be dependent on the EB diameter, as usually thought, but on the total cell number in the EB. Both in hanging drop and the device methods, cardiogenesis was maximized when 17,000 cells aggregated to form the EB; however, the diameters of the aggregates differed by almost 50 μm. Cardiomyocyte production is significantly lower when the cell number is either increased or decreased, independent of the characteristics of the EB (Supplementary Table S1, Supplementary Fig. S8).

EB aggregates produced by any method usually show beating areas from day 5 onward [40]. In our experiments, EBs created by hanging drops showed beating areas on day 7 onwards, while EBs extracted from the device started beating a day later. The health of the functional (i.e., beating) cardiomyocytes and the presence of beating areas were analyzed using the tools developed by Huebsch, N et al. [41] to measure the frequencies and displacements of beating cell cultures using Kalman filtering [42]. Briefly, the system works by analyzing consecutive images of a pulsating culture and calculating beating frequency, amplitude, and direction, identifying the centers of motion (i.e., source of contraction) based on the displacement of the surrounding cells. The results of this analysis are shown in (Fig. 4A–D) (Supplementary Fig. S5).

The results show that EBs produced from the micro-aggregation chamber shows the overall controlled contraction pattern characteristic of healthy and stable tissue; The cardiac cells are metabolically active and indicative of developing cardiomyocytes because of the rhythmic contraction due to the cytosolic glycolysis pathway [43]. Irrespective to

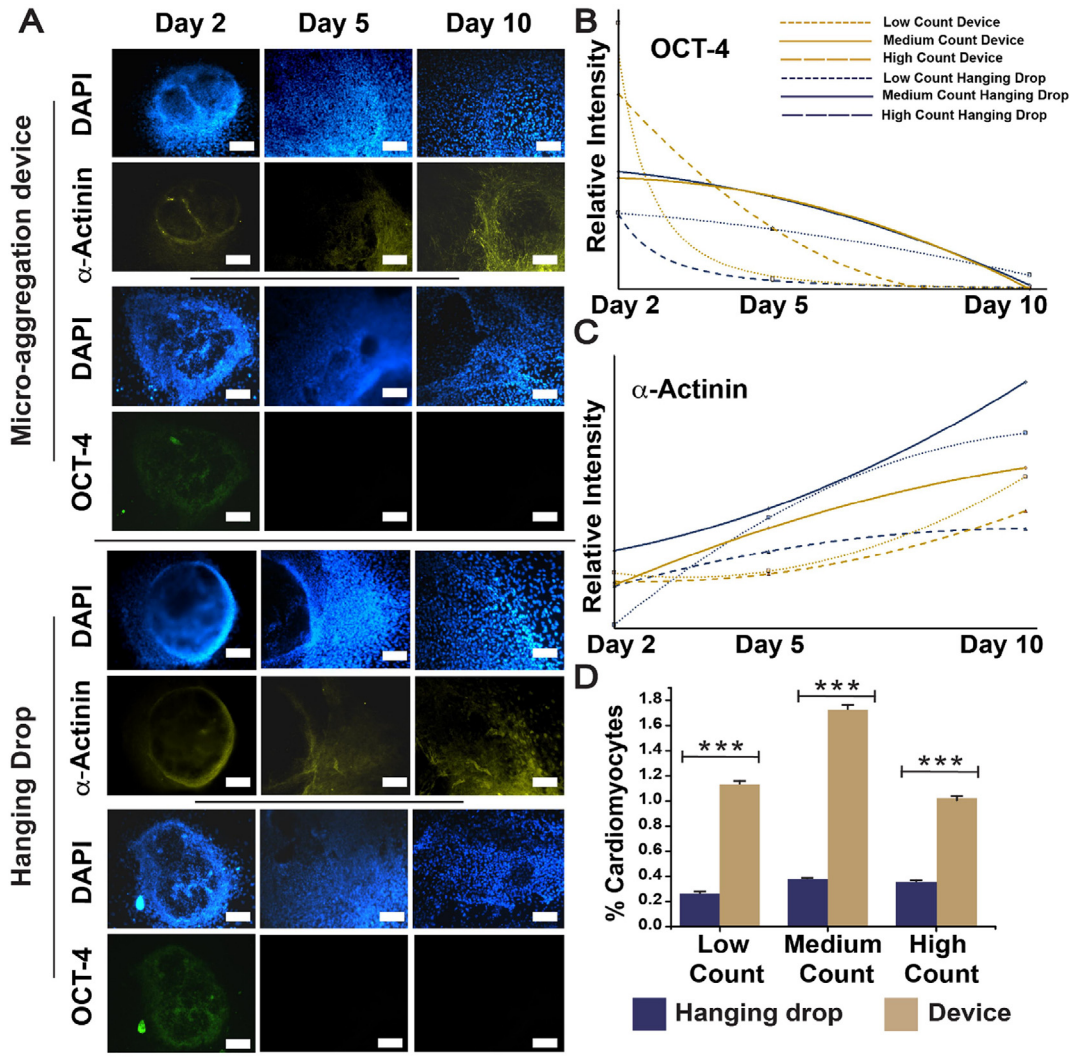

Fig. 3. Qualitative analysis differentiation and pluripotency markers by Immunostaining study. (A) The EBs extracted from the micro-aggregation device and the hanging drop cultures were studied over a span of 10days to monitor the expression α-Sarcomeric Actinin and OCT-4(Scale: 100 μm) (Supplementary Fig. S6) has shows higher magnification images of the expressing protein markers. (B) A pattern of upregulation was seen in α-Sarcomeric Actinin indicating EB differentiation extracted from both the techniques (small dash represents low count, solid lines represent medium count and big dash represents high count of cells). (C) Similarly, OCT-4 which is the pluripotency marker was also monitored and there was a significant decrease in the expression level observed post day 5 of the development (graphical annotation for representing downregulation of OCT-4 is the same as mentioned above). (D)Statistical analysis of the flow cytometry data depicting the amounts of cardiomyocytes produced from the two different technique used for the study.

the cell number present the beating frequency was unaltered for the EBs extracted from the micro-aggregation chamber whereas for the hanging drop culture method harvested EBs; the beats/min is higher for the low cell count followed by plateauing in medium and high cell count. The reason of this phenomenon can be explained by fluctuation-dissipation theorem, stating that stable cardiomyocytes are like a heavy mass pendulum which is not affected by any internal or external perturbations [44]. In contrast, unstable cardiomyocytes tend to beat at a faster rhythm as they are affected by the neighboring cell properties, which explains the higher beating rate in hanging drop derived low cell count cardiac cells. The functionality of the cardiomyocytes competes with the best results obtained by traditional techniques in the past [45] and is similar to the characteristics of cardiomyocytes in vivo [46], reflecting the applicability of the de novo cells in medical therapies [47]. Therefore, the fine control of the SC aggregation in the proposed chip enabled the production of cardiomyocytes of similar quality to current technologies but with effectiveness over four times higher in their production.

4. Summary and conclusion

In summary, cardiomyocyte production from embryonic stem cells was used as a basis to show the possibility of combining two aspects of science together: stem cell research and digital manufacturing. These findings highlight the possibility of using the increasing precision of additive manufacturing to address the limitations of some biological methods—specifically for stem cell differentiation.

We show that high-precision 3D micro-fabrication enables the formation of embryoid bodies of unparalleled uniformity in size and geometry, thereby leading to higher percentages of cardiomyocyte production.

The results shown here are the initial demonstration of the possibilities that 3D printing brings to stem cell biology, linking the continuous enhancement of precision in 3D printing with a higher control on cell differentiation. Additionally, they open new and exciting perspectives for the field; As the technology proposed here follows a “bioinspired” approach—making use of only cell-cell communication as the

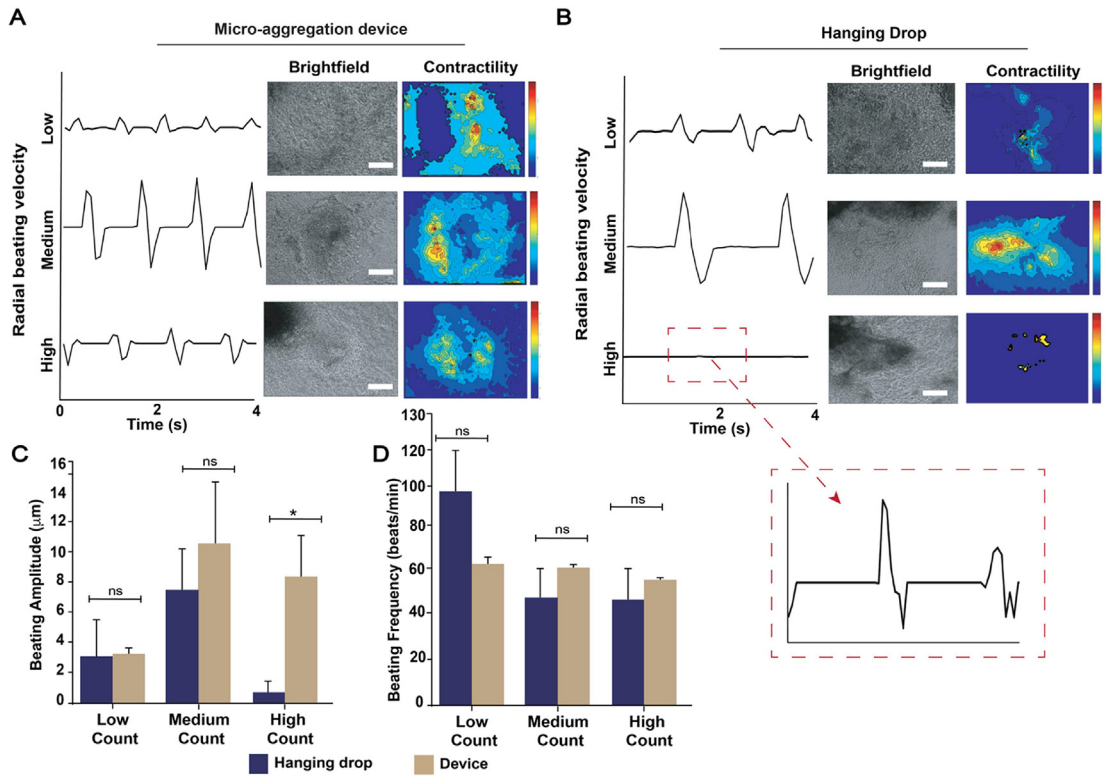

Fig. 4. Cardiac tissue health determination (A) Representation of the cardiogram and center of contraction of the cardiac cells produced by the EBs extracted from the micro-aggregation device containing different cell number aggregates (Scale: 200 μm). (B) Showing the cardiogram and center of contraction of the cardiac cells produced by the EBs extracted from the hanging drop cultures (Scale: 200 μm). (C–D) Statistical measurement of the beating intensity plotted in terms of frequency and amplitude.

differentiation factor, it avoids the limitations of those methods based on exogenous factors, where all cells are equally influenced by the differentiating factors. Therefore, the use of the bioinspired approach over the chemical methods for differentiation gives a cutting edge advantage in the technologically advanced biomedical community; the method adopted here carries the potential to mimic the complexity of a developing embryo in vivo (e.g. the formation of an entire organ post differentiation) instead of forcibly pushing all the cells into one particular lineage. The novelty of this system can thus be used to condition the stem cells into cardiomyocytes and study the drug response, disease modelling, and regenerative medicine.

Statistical analysis

Comparison between the groups were made by Student's t-tests. All the results here are shown as mean ± standard error (S.E.M.). The significance was predetermined at $P < 0.05$.

Data and materials availability

Data supporting the findings of this study are available within the article and its supplementary information files, and also from the corresponding author upon reasonable request.

CRediT authorship contribution statement

Rupambika Das: Data curation, Experimentation, Image Preparation, Conceptualization, Methodology, Writing - original draft. **Javier G. Fernandez:** Conceptualization, Methodology, Writing - original draft, Supervision, Writing - review & editing.

Declaration of competing interest

The authors declare that they have no known competing financial interests or personal relationships that could have appeared to influence the work reported in this paper.

Acknowledgments

General: We thank Dr. Norris Ray Dunn (IMB, A-star) for providing us with stem cells for carrying out the studies. This research has been funded by the SUTD-MIT International Design Center (IDC).

Appendix A. Supplementary data

Supplementary data to this article can be found online at https://doi.org/10.1016/j.bprint.2020.e00091.

References

[1] A. Leri, M. Rota, F.S. Pasqualini, P. Goichberg, P. Anversa, Origin of cardiomyocytes in the adult heart, Circ. Res. 116 (1) (2015) 150–166.
[2] K. Kikuchi, J.E. Holdway, A.A. Werdich, R.M. Anderson, Y. Fang, G.F. Egnaczyk, T. Evans, C.A. MacRae, D.Y. Stainier, K.D. Poss, Primary contribution to zebrafish heart regeneration by gata4+ cardiomyocytes, Nature 464 (7288) (2010) 601.
[3] A.P. Beltrami, K. Urbanek, J. Kajstura, S.-M. Yan, N. Finato, R. Bussani, B. Nadal-Ginard, F. Silvestri, A. Leri, C.A. Beltrami, Evidence that human cardiac myocytes divide after myocardial infarction, N. Engl. J. Med. 344 (23) (2001) 1750–1757.
[4] A. Leri, J. Kajstura, P. Anversa, Cardiac Regeneration and Aging, Heart Development and Regeneration, Elsevier, 2010, pp. 951–980.
[5] S. Akhtar, Ischemic heart disease, Anesthesiol. Clin. 24 (3) (2006) 461–485.
[6] K. Thygesen, J.S. Alpert, A.S. Jaffe, M.L. Simoons, B.R. Chaitman, H.D. White, Joint ESC/ACCF/AHA/WHF Task Force for the Universal Definition of Myocardial Infarction, Third universal definition of myocardial infarction, Eur. Heart J. 33 (20) (2012) 2551–2567.
[7] W.J. Richardson, S.A. Clarke, T.A. Quinn, J.W. Holmes, Physiological implications of myocardial scar structure, Comprehen. Physiol. 5 (4) (2011) 1877–1909.

[8] E. Struck, S. Hagl, H. Meisner, F. Sebening, Heart transplantation: limitations and perspectives, Zeitschrift fur Kardiologie 74 (1985) 59–63.
[9] K.R. Boheler, J. Czyz, D. Tweedie, H.-T. Yang, S.V. Anisimov, A.M. Wobus, Differentiation of pluripotent embryonic stem cells into cardiomyocytes, Circ. Res. 91 (3) (2002) 189–201.
[10] H. Rippon, A. Bishop, Embryonic stem cells, Cell Prolif 37 (1) (2004) 23–34.
[11] P.J. Donovan, J. Gearhart, The end of the beginning for pluripotent stem cells, Nature 414 (6859) (2001) 92.
[12] E. Winter, A. Gittenberger-de Groot, Cardiovascular development: towards biomedical applicability, Cell. Mol. Life Sci. 64 (6) (2007) 692–703.
[13] M.A. Kinney, R. Saeed, T.C. McDevitt, Systematic analysis of embryonic stem cell differentiation in hydrodynamic environments with controlled embryoid body size, Integrative Biol 4 (6) (2012) 641–650.
[14] J.M. Kim, S.-H. Moon, S.G. Lee, Y.J. Cho, K.S. Hong, J.H. Lee, H.J. Lee, H.-M. Chung, Assessment of differentiation aspects by the morphological classification of embryoid bodies derived from human embryonic stem cells, Stem Cell. Dev. 20 (11) (2011) 1925–1935.
[15] M.Y. Lee, E.C. Bozkulak, S. Schliffke, P.J. Amos, Y. Ren, X. Ge, B.E. Ehrlich, Y. Qyang, High density cultures of embryoid bodies enhanced cardiac differentiation of murine embryonic stem cells, Biochem. Biophys. Res. Commun. 416 (1) (2011) 51–57.
[16] Y.-S. Hwang, B.G. Chung, D. Ortmann, N. Hattori, H.-C. Moeller, A. Khademhosseini, Microwell-mediated control of embryoid body size regulates embryonic stem cell fate via differential expression of WNT5a and WNT11, Proc. Natl. Acad. Sci. U. S. A 106 (40) (2009) 16978–16983.
[17] J. Antonchuk, Formation of Embryoid Bodies from Human Pluripotent Stem Cells Using AggreWell™ Plates, Basic Cell Culture Protocols, Springer, 2013, pp. 523–533.
[18] M. Kibschull, Differentiating mouse embryonic stem cells into embryoid bodies in AggreWell plates, Cold Spring Harb. Protoc. 6 (2017) (2017) pdb. prot094169.
[19] H. Kurosawa, Methods for inducing embryoid body formation: in vitro differentiation system of embryonic stem cells, J. Biosci. Bioeng. 103 (5) (2007) 389–398.
[20] R. Foty, A simple hanging drop cell culture protocol for generation of 3D spheroids, JoVE: JoVE 51 (2011).
[21] M.D. Ungrin, C. Joshi, A. Nica, C. Bauwens, P.W. Zandstra, Reproducible, ultra high-throughput formation of multicellular organization from single cell suspension-derived human embryonic stem cell aggregates, PloS One 3 (2) (2008) e1565.
[22] J.C. Mohr, J. Zhang, S.M. Azarin, A.G. Soerens, J.J. de Pablo, J.A. Thomson, G.E. Lyons, S.P. Palecek, T.J. Kamp, The microwell control of embryoid body size in order to regulate cardiac differentiation of human embryonic stem cells, Biomaterials 31 (7) (2010) 1885–1893.
[23] J.C. Waters, Accuracy and precision in quantitative fluorescence microscopy, J. Cell Biol. 185 (7) (2009) 1135–1148.
[24] J. Park, C.H. Cho, N. Parashurama, Y. Li, F. Berthiaume, M. Toner, A.W. Tilles, M.L. Yarmush, Microfabrication-based modulation of embryonic stem cell differentiation, Lab Chip 7 (8) (2007) 1018–1028.
[25] J.M. Karp, J. Yeh, G. Eng, J. Fukuda, J. Blumling, K.-Y. Suh, J. Cheng, A. Mahdavi, J. Borenstein, R. Langer, Controlling size, shape and homogeneity of embryoid bodies using poly (ethylene glycol) microwells, Lab Chip 7 (6) (2007) 786–794.
[26] X. Wang, P. Yang, In vitro differentiation of mouse embryonic stem (mES) cells using the hanging drop method, JoVE (17) (2008), e825.
[27] P.W. Burridge, D. Anderson, H. Priddle, M.D. Barbadillo Munoz, S. Chamberlain, C. Allegrucci, L.E. Young, C. Denning, Improved human embryonic stem cell embryoid body homogeneity and cardiomyocyte differentiation from a novel V-96 plate aggregation system highlights interline variability, Stem Cell. 25 (4) (2007) 929–938.
[28] S. Knowlton, C.H. Yu, F. Ersoy, S. Emadi, A. Khademhosseini, S. Tasoglu, 3D-printed microfluidic chips with patterned, cell-laden hydrogel constructs, Biofabrication 8 (2) (2016), 025019.
[29] J. Bortman, F. Mahmood, M. Schermerhorn, R. Lo, N. Swerdlow, F. Mahmood, R. Matyal, Use of three-dimensional printing to create patient-specific abdominal aortic aneurysm models for pre-operative planning, J. Cardiothorac. Vasc. Anesth. 33 (5) (2019) 1442–1446.
[30] C.A. Mills, J.G. Fernandez, E. Martinez, M. Funes, E. Engel, A. Errachid, J. Planell, J. Samitier, Directional alignment of MG63 cells on polymer surfaces containing point microstructures, Small 3 (5) (2007) 871–879.
[31] W. Gao, Y. Zhang, D. Ramanujan, K. Ramani, Y. Chen, C.B. Williams, C.C. Wang, Y.C. Shin, S. Zhang, P.D. Zavattieri, The status, challenges, and future of additive manufacturing in engineering, Comput. Aided Des. 69 (2015) 65–89.
[32] K.J. Regehr, M. Domenech, J.T. Koepsel, K.C. Carver, S.J. Ellison-Zelski, W.L. Murphy, L.A. Schuler, E.T. Alarid, D.J. Beebe, Biological implications of polydimethylsiloxane-based microfluidic cell culture, Lab Chip 9 (15) (2009) 2132–2139.
[33] J.G. Fernandez, J. Samitier, C.A. Mills, Simultaneous biochemical and topographical patterning on curved surfaces using biocompatible sacrificial molds, J. Biomed. Mater. Res. 98A (2) (2011) 229–234.
[34] J.G. Fernandez, C.A. Mills, M. Pla-Roca, J. Samitier, Forced Soft Lithography (FSL): production of micro- and nanostructures in thin freestanding sheets of Chitosan biopolymer, Adv. Mater. 19 (21) (2007) 3696–3701.
[35] L.J. Millet, M.U. Gillette, Over a century of neuron culture: from the hanging drop to microfluidic devices, Yale J. Biol. Med. 85 (4) (2012) 501.
[36] C.J. Fuegemann, A.K. Samraj, S. Walsh, B.K. Fleischmann, S. Jovinge, M. Breitbach, Differentiation of mouse embryonic stem cells into cardiomyocytes via the hanging-drop and mass culture methods, Currnt. Protocol. Stem Cell. Biol 15 (1) (2010), 1F. 11.1-1F. 11.13.
[37] M. Tewary, D. Dziedzicka, J. Ostblom, L. Prochazka, N. Shakiba, C. Woodford, E. Piccinini, A. Vickers, B. Louis, N. Rahman, High-throughput micro-patterning platform reveals Nodal-dependent dissection of peri-gastrulation-associated versus pre-neurulation associated fate patterning, BioRxiv (2018) 465039.
[38] S.-H. Moon, J. Ju, S.-J. Park, D. Bae, H.-M. Chung, S.-H. Lee, Optimizing human embryonic stem cells differentiation efficiency by screening size-tunable homogenous embryoid bodies, Biomaterials 35 (23) (2014) 5987–5997.
[39] G.J. Scuderi, J. Butcher, Naturally engineered maturation of cardiomyocytes, Front. Cell. Dev. Biol 5 (2017) 50.
[40] C. Mummery, D. Ward, C. Van Den Brink, S. Bird, P. Doevendans, T. Opthof, A.B. De La Riviere, L. Tertoolen, M. Van Der Heyden, M. Pera, Cardiomyocyte differentiation of mouse and human embryonic stem cells, J. Anat. 200 (3) (2002) 233–242.
[41] N. Huebsch, P. Loskill, M.A. Mandegar, N.C. Marks, A.S. Sheehan, Z. Ma, A. Mathur, T.N. Nguyen, J.C. Yoo, L.M. Judge, Automated video-based analysis of contractility and calcium flux in human-induced pluripotent stem cell-derived cardiomyocytes cultured over different spatial scales, Tissue Eng. C Methods 21 (5) (2015) 467–479.
[42] Y. Zheng, S. Chen, W. Tan, R. Kinnick, J.F. Greenleaf, Detection of tissue harmonic motion induced by ultrasonic radiation force using pulse-echo ultrasound and Kalman filter, IEEE Trans. Ultrason. Ferroelectrics Freq. Contr. 54 (2) (2007).
[43] S. Malandraki-Miller, C.A. Lopez, H. Al-Siddiqi, C.A. Carr, Changing metabolism in differentiating cardiac progenitor cells—can stem cells become metabolically flexible cardiomyocytes? Fronti. Cardiovasc. Med. 5 (2018) 119.
[44] T. Hayashi, T. Tokihiro, H. Kurihara, K. Yasuda, Community effect of cardiomyocytes in beating rhythms is determined by stable cells, Sci. Rep. 7 (1) (2017) 15450.
[45] B.S. Yoon, S.J. Yoo, J.E. Lee, S. You, H.T. Lee, H.S. Yoon, Enhanced differentiation of human embryonic stem cells into cardiomyocytes by combining hanging drop culture and 5-azacytidine treatment, Differentiation 74 (4) (2006) 149–159.
[46] K. Rajala, M. Pekkanen-Mattila, K. Aalto-Setälä, Cardiac differentiation of pluripotent stem cells, Stem Cell. Int. 2011 (2011).
[47] P.W. Burridge, G. Keller, J.D. Gold, J.C. Wu, Production of de novo cardiomyocytes: human pluripotent stem cell differentiation and direct reprogramming, Cell stem cell 10 (1) (2012) 16–28.